HHS Public Access

Author manuscript

Gastro Hep Adv. Author manuscript; available in PMC 2023 June 11.

Published in final edited form as:

Gastro Hep Adv. 2022 ; 1(4): 682–697. doi:10.1016/j.gastha.2022.02.007.

Eicosanoids in the pancreatic tumor microenvironment – a multicellular, multifaceted progression

Vikas B. Gubbala[1], **Nidhi Jytosana**[2], **Vincent Q. Trinh**[3], **H. Carlo Maurer**[4,11], **Razia F. Naeem**[1], **Nikki K. Lytle**[1], **Zhibo Ma**[1], **Steven Zhao**[5], **Wei Lin**[6], **Haiyong Han**[6], **Yu Shi**[7,^], **Tony Hunter**[7], **Pankaj K. Singh**[8], **Kenneth P. Olive**[4], **Marcus C.B. Tan**[3,9,10], **Susan M. Kaech**[5], **Geoffrey M. Wahl**[1,*], **Kathleen E. DelGiorno**[2,9,10,*]

[1]Gene Expression Laboratory, Salk Institute for Biological Studies, La Jolla, CA, 92037

[2]Department of Cell and Developmental Biology, Vanderbilt University, Nashville, TN, 37232

[3]Department of Surgery, Vanderbilt University Medical Center, Nashville, TN, 37232

[4]Department of Medicine, Herbert Irving Comprehensive Cancer Center, Columbia University Irving Medical Center, New York, NY, 10032

[5]Immunobiology and Microbial Pathogenesis Laboratory, Salk Institute for Biological Studies, La Jolla, CA, 92037

[6]Molecular Medicine Division, Translational Genomics Research Institute, Phoenix, AZ, 85004

[7]Molecular and Cell Biology Laboratory, Salk Institute for Biological Studies, La Jolla, CA, 92037,

[8]Eppley Institute for Research in Cancer, University of Nebraska Medical Center, Omaha, NE, 68198

[9]Vanderbilt Digestive Disease Research Center, Vanderbilt University Medical Center, Nashville, TN, 37232

[10]Vanderbilt Ingram Cancer Center, Nashville, TN, 37232

[11]Internal Medicine II, School of Medicine, Technische Universität München, Munich, Germany

Abstract

[*]Correspondence to: Kathleen E. DelGiorno (kathleen.delgiorno@vanderbilt.edu) and Geoffrey M. Wahl (wahl@salk.edu).
[^]Current address: Bristol Myers Squibb, R&D, San Diego, CA, USA

Author contributions: Conceptualization: K.E.D. Formal analysis: V.B.G., N.J., V.Q.T., Z.M., H.C.M., W.L., P.K.S., K.E.D. Funding acquisition: H.H., T.H., P.K.S., S.M.K., K.P.O., G.M.W., K.E.D. Investigation: V.B.G., N.J., V.Q.T., R.F.N., N.K.L., C.H.M., S.Z., W.L., Y.S., K.E.D. Project administration: K.E.D. Resources: H.C.M., W.L., H.H., Y.S., T.H., K.P.O. Supervision: H.H., T.H., M.C.B.T., P.K.S., S.M.K., K.P.O., G.M.W., K.E.D. Visualization: V.B.G., K.E.D. Writing: V.B.G., G.M.W., K.E.D.

Data Transparency Statement: All data are included in this manuscript.

Conflicts of interest: The authors disclose no conflicts.

Ethical Statement: The corresponding author, on behalf of all authors, jointly and severally, certifies that their institution has approved the protocol for any investigation involving humans or animals and that all experimentation was conducted in conformity with ethical and humane principles of research.

Background and Aims: Eicosanoids, oxidized fatty acids that serve as cell-signaling molecules, have been broadly implicated in tumorigenesis. Here, we aimed to identify eicosanoids associated with pancreatic tumorigenesis and the cell types responsible for their synthesis.

Methods: We profiled normal pancreas and pancreatic ductal adenocarcinoma (PDAC) in mouse models and patient samples using mass spectrometry. We interrogated RNA sequencing datasets for eicosanoid synthase or receptor expression. Findings were confirmed by immunostaining.

Results: In murine models, we identified elevated levels of PGD_2, prostacyclin, and thromboxanes in neoplasia while PGE_2, 12-HHTre, HETEs, and HDoHEs are elevated specifically in tumors. Analysis of scRNA-seq datasets suggests that PGE_2 and prostacyclins are derived from fibroblasts, PGD_2 and thromboxanes from myeloid cells, and PGD_2 and 5-HETE from tuft cells. In patient samples, we identified a transition from PGD_2 to PGE_2-producing enzymes in the epithelium during the transition to PDAC, fibroblast/tumor expression of PTGIS, and myeloid/tumor cell expression of TBXAS1.

Conclusions: Our analyses identify key changes in eicosanoid species during pancreatic tumorigenesis and the cell types that contribute to their synthesis. Thromboxane and prostacyclin expression is conserved between animal models and human disease and may represent new druggable targets.

Graphical Abstract

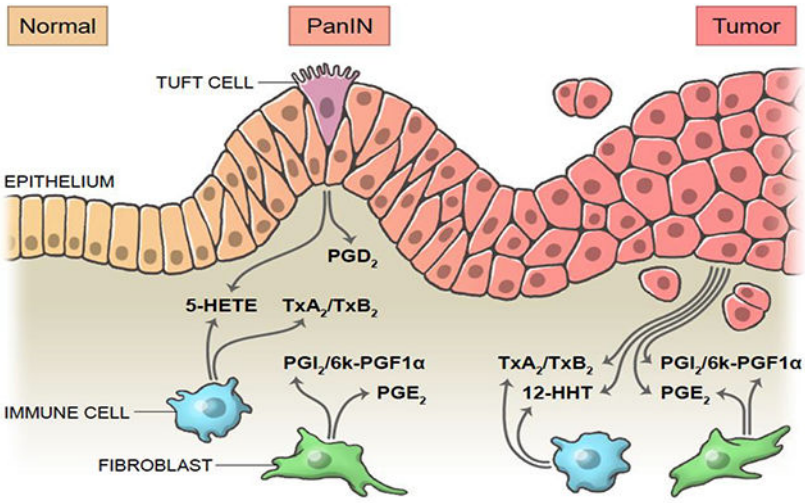

Keywords

tuft cells; prostaglandins; PTGES; PTGIS; TBXAS1

Introduction

Pancreatic ductal adenocarcinoma (PDAC) can arise from the progression of acinar-to-ductal metaplasia through several grades of pancreatic intraepithelial neoplasia (PanINs), which are characterized by increasing nuclear atypia and loss of cellular polarity. Metaplasia is a process in which acinar cells transdifferentiate into ductal-like cells in response to pancreatic

damage to re-establish homeostasis. However, in the context of oncogenic mutations, such as *Kras*^{G12D}, ADM becomes irreversible and leads to the formation of hyperplastic ductal structures known as PanINs. Accumulation of additional genetic mutations leads to tumor formation[1]. Interestingly, ADM does not result in the formation of a homogeneous population of cells. Instead, ADM generates diverse, differentiated, secretory cells, including tuft cells. Tuft cells, or solitary chemosensory cells, have been detected in chronic pancreatitis and *Kras*^{G12D}-induced tumorigenesis[2, 3]. Recently, we showed that tuft cells attenuate pancreatic tumorigenesis through the synthesis and secretion of the eicosanoid prostaglandin D_2 (PGD_2)[4]. These cells, which are proposed to play diverse roles in early tumorigenesis and immune cell recruitment, are abundant in preinvasive lesions but are lost in the adenocarcinoma stage of pancreatic tumorigenesis[2].

Cellular crosstalk within the tumor microenvironment can significantly affect tumor progression. One important class of signaling molecules involved in this crosstalk are eicosanoids, or lipid products derived from the enzymatic or non-enzymatic oxidation of polyunsaturated fatty acids (PUFAs)[5]. Hundreds of eicosanoids have been characterized, each with distinct, context dependent roles based on the presence and characteristics of receptors expressed in the tumor microenvironment. Eicosanoids can be further subdivided into broad classes – including prostanoids, HETEs, and HdoHEs – based on the precursor molecule PUFA and the synthases responsible for their production.

Arachidonic acid is a common precursor for many different eicosanoids and certain phospholipases (PLA2G2A, PLA2G4A) can generate arachidonic acid from membrane phospholipids. Synthesis of prostanoid-type eicosanoids begins with metabolism of arachidonic acid by cyclooxygenases (COX1, COX2), to prostaglandin G_2 (PGG_2), which is non-enzymatically metabolized to prostaglandin H_2 (PGH_2). Terminal synthases are required to convert this substrate to specific prostanoid molecules (Figure 1A)[5, 6].

Prostanoids have been studied in the context of tumorigenesis in a variety of organ systems. Prostaglandin E_2 (PGE_2) has been linked to tumor growth, metastasis, and fibroblast function in several cancers including PDAC[5, 7, 8]. Its metabolite, dhk-PGE_2, is generated by the enzyme HPGD (also known as 15-PGDH); HPGD ablation has been shown to accelerate tumorigenesis in the intestines and pancreas[9, 10]. Prostaglandin D_2 (PGD_2) can suppress tumor cell proliferation and metastasis in intestinal adenomas and gastric cancer[11, 12]. Thromboxane A_2 (TxA_2) typically functions as a platelet activator and vasoconstrictor but has also been implicated in promoting tumor cell growth, metastasis, and regulation of neovascularization in breast cancer, lung cancer and more[13–15]. TxA_2 has a very short half-life and quickly metabolizes to thromboxane B_2 (TxB_2), a product predicted to have minimal biological activity[16]. Produced in equimolar ratios in thromboxane biosynthesis is prostaglandin 12-HHTre, a relatively understudied eicosanoid with only one known receptor, BLT2 (*LTB4R2*)[17]. 12-HHTre can also be produced by cytochrome proteins, such as CYP2S1[18]. Although prostacyclin (PGI_2) antagonizes the actions of TxA_2 and acts as a vasodilator and inhibitor of platelet activation, it too has been implicated in pro-tumorigenic, pro-angiogenic roles in the tumor microenvironment and is associated with poor prognosis in lung, ovarian, and gastric cancers[19, 20]. It also has a short half-life, and readily breaks down into the inert, stable product 6k-$PGF1\alpha$[21].

Lipoxygenases oxidize arachidonic acid to generate HETEs (Figure 1B)[22–24]. 5-HETE is generated from 5-lipoxygenase (ALOX5); ALOX5 inhibition has been shown to slow the growth of cancer cells *in vitro*[25–27]. The role of eicosanoid 15-HETE, on the other hand, is less clear, as it has been implicated in both pro- and anti-tumorigenic roles[28, 29]. Lipoxygenases can metabolize the PUFA docosahexaenoic acid (DHA) into HDoHEs (14-HDoHE, 17-HDoHE), biosynthetic precursors to maresins and D-resolvins, respectively[30, 31]. While the action(s) of HDoHEs in cancer are unknown, their metabolic byproducts can attenuate inflammation and wound healing and maresins can inhibit tumor growth[32].

Broad inhibition of prostanoid synthesis by targeting the upstream synthase COX2 has been shown to reduce tumor growth and metastasis, reverse collagen deposition, sensitize tumors to immunotherapy, normalize the vasculature, and enhance the response to chemotherapy in mouse models[7, 33, 34]. However, COX2 inhibition blocks the synthesis of several downstream eicosanoids, causing significant off-target effects. To develop better, more specific therapeutics, it is important to characterize eicosanoid diversity in PDAC. To accomplish this, we conducted eicosanoid profiling on normal pancreata and PDAC in mouse models of pancreatic tumorigenesis and human patient samples. We then interrogated published scRNA-seq datasets to identify the cellular source(s) of eicosanoid synthases and receptors and validated key findings at the protein level.

Methods

Mice.

Mice were housed in accordance with NIH guidelines in AAALAC-accredited facilities at the Salk Institute for Biological Studies. The Salk Institute IACUC approved all animal studies. *LSL-Kras*$^{G12D/+}$, *Ptf1a*$^{Cre/+}$, *Pdx1Cre*, *Trp53*^{R17H}, and *Trp53*$^{fl/fl}$ mice have previously been described[35, 36]. C57B6/J mice were either purchased from the Jackson Laboratory (Bar Harbor, ME) or bred in-house. CD1 mice were either purchased from Charles River Laboratories (Wilmington, MA) or bred in-house.

Human samples.

Distribution and use of all human samples was approved by the Institutional Review Boards of the Salk Institute for Biological Studies and Vanderbilt University. Flash frozen human pancreas samples were either purchased from Indivumed (Frederick, MD) or were acquired from the Cooperative Human Tissue Network (CHTN). All normal pancreas samples were acquired from PDAC patients and were pathologically determined to be normal.

Comprehensive eicosanoid panel.

Eicosanoid profiling was conducted on flash-frozen pancreas tissue from wild type mice (C57B6/J or CD1), *KPC* mice, or orthotopic tumors (cell lines FC-1199, FC-1242, and FC-1245) grown in C57B6/J mice. In separate experiments, eicosanoid profiling was performed on flash frozen human PDAC or normal pancreas. Age-matched normal and PanIN-bearing pancreata were included from a previous study[4]. Tissues were homogenized in 1 ml of PBS containing 10% ethanol and 300 μl were extracted using strata-x polymeric

reverse phase columns (88-S100-UBJ Phenomenex). Samples were taken up in 50 μl of 63% H_20, 37% ACN, 0.02% Acetic Acid, and 10 μl was injected into UPLC (ACQUITY UPLC System, Waters) and analyzed on a Sciex 6500 Qtrap mass spectrometer at the UCSD Lipidomics Core as previously described[37]. Tissue eicosanoid concentrations were quantified using deuterated internal standards in conjunction with standard curves obtained in parallel using identical conditions as previously described[38], and were normalized to total protein mass of the sample.

Statistical analysis.

Statistical analyses, data processing, heatmap plotting, hierarchical clustering, and PCA analysis were performed in R (https://www.r-project.org/) and/or Prism (GraphPad). Statistical significance was calculated by either two-tailed unpaired t-tests assuming equal variance or one-way ANOVA. qRT-PCR and IHC quantification data are expressed as mean ± standard deviation. Eicosanoid levels are expressed as mean ± standard error of the mean.

Results

Eicosanoid composition evolves throughout pancreatic tumorigenesis

To broadly profile eicosanoid diversity, we used mass spectrometry and assessed a panel of over 157 eicosanoid species in normal pancreata, autochthonous tumors from either *Kras*^{G12D};*Trp53*^{R172H};*Ptf1a*$^{Cre/+}$ or *Kras*^{G12D};*Trp53*$^{fl/fl}$,*Pdx1-Cre* mice (collectively referred to as *KPC*) and syngeneic orthotopic tumors generated from 3 separate PDAC cell lines (derived from *KPC* mice) (Figure S1A, File S1). We identified significant increases in mean concentration for several eicosanoids in autochthonous *KPC* tumors (n = 11) as compared to normal pancreata (n = 9) (Figure 1C, mean difference > 20 pmol/mg protein, $p < 0.05$). Most of the elevated species belong to the prostaglandin class of eicosanoids, including PGE_2 and its metabolite dhk-PGE_2, PGD_2, thromboxane synthesis byproducts 12-HHTrE and TxB_2, and prostacyclin (PGI_2) metabolite 6k-PGF1α (Figure 1A, 1C). Other eicosanoids identified in *KPC* tumors are lipoxygenase-derived HETEs (5-HETE, 11-HETE, 15-HETE) and docosahexaenoic acid derived HDoHEs (14-HDoHE, 17-HDoHE, 8-HDoHE) (Figure 1B–C). To determine if eicosanoid levels in orthotopically generated PDAC tumors reflect those identified in autochthonous models, we analyzed tumors generated from three different murine PDAC cell lines (FC-1199, FC-1242, and FC-1245, n = 3/line). Interestingly, most eicosanoids identified as elevated in autochthonous models, relative to normal pancreas, were also elevated in orthotopic tumors except for 5-HETE (Figure 1D). Additionally, analysis of orthotopic tumor profiles identified a significant decrease in linoleic acid oxidation products 9- and 13-oxoODE, as compared to normal pancreas, which did not reach significance in autochthonous PDAC tumor profiles (Figure 1D).

Previously, we profiled eicosanoid species in normal and PanIN-bearing pancreata from 8–10 month old *Kras*^{G12D};*Ptf1a*$^{Cre/+}$ (*KC*) mice (n = 5) and discovered significant upregulation of several eicosanoids, including TxB_2, 6k-PGF1α, and PGD_2; 5-HETE was found to be elevated but did not reach significance (Figure 1E)[4]. To determine how eicosanoid species and levels change between pre-invasive PanIN and PDAC, we compared these data to the profiles we generated for *KPC* tumors. We observed a statistically significant gain in

prostaglandins TxB_2, 12-HHTrE, 6k-PGF1α, PGE_2, and 8-HDoHE in tumors as compared to PanIN (Figure 1F). Interestingly, 12-HHTre appears to be tumor-specific. We next examined eicosanoid patterns across all the profiled samples using hierarchical clustering of select eicosanoids (Figure 1G). While normal samples clustered tightly and displayed low levels of selected eicosanoids, murine tumors displayed a large degree of heterogeneity, consistent with heterogeneity observed in tumorigenesis and stromal deposition in these models[35, 36]. Notably, orthotopic tumors clustered by cell line, with those derived from FC-1199 displaying a trend towards increased eicosanoid production as compared to FC-1242 and FC-1245. While autochthonous tumors displayed an overall higher level of the selected eicosanoids, several samples clustered closer to orthotopic tumor samples. The five profiled PanIN samples displayed sample-to-sample heterogeneity, consistent with disease progression in this model, but were characterized by intermediate levels of select eicosanoids (Figure 1G)[39].

Altogether, these analyses identify classes of eicosanoids that are altered during pancreatic tumorigenesis. Specifically, several prostaglandins (PGE_2, PGD_2, TxB_2, 12-HHTrE, 6k-PGF1α), HETEs, and HDoHEs are upregulated in murine tumor models in a relatively consistent manner, although there is heterogeneity within and between commonly used PDAC models (Figure 1H).

Cell type-specific expression of eicosanoid synthases and receptors in murine PanIN

In our eicosanoid profiling studies, we identified significant changes in several eicosanoid species during pancreatic tumorigenesis (Figure 1G). As pancreas cellular composition changes with disease progression, the relative contribution of each of these various cell types (i.e., epithelium, inflammatory cells, fibroblasts) to eicosanoid production likely changes as well. To identify these changes, we examined available single cell RNA sequencing (scRNA-seq) datasets generated from murine models of PanIN and PDAC. We focused our analyses on eicosanoid synthases and receptors with well-defined biosynthetic pathways, including prostaglandins and lipoxygenases.

Schlesinger et al., recently generated an extensive scRNA-seq dataset comprised of 43,897 cells encompassing epithelial and stromal cell types from 9 $Kras^{G12D};Ptf1aCre^{ERTM/+};Rosa26^{LSL\text{-}tdTomato/+}$ mice at various stages of disease progression[40]. To identify major cellular sources of eicosanoid synthesis, we reanalyzed the Schlesinger dataset. As shown in Figure 2A, sequence libraries were combined, and clusters were annotated by examining both classic cell type markers and previously published single-cell gene signatures (Figure S1B)[41]. As several time-points were included in this dataset, normal pancreas cells, preinvasive cells (including tuft cells), and tumor cells are represented. We first examined expression of upstream synthases in the prostaglandin synthesis pathway. We detected expression of phospholipase *Pla2g4a* in epithelial cells - including pre-invasive cells and tuft cells - as well as in stromal cells such as fibroblasts (Figure 2B). The cyclooxygenases *Ptgs1* (COX1) and *Ptgs2* (COX2) are co-expressed in macrophages, fibroblasts, and tuft cells (as previously described)[2]. *Ptgs1* is additionally expressed in endothelial cells and several immune cell types (Figure 2B–C). We next examined expression of terminal prostaglandin synthases and identified macrophages and

tuft cells to be major sources of the PGD_2 synthase *Hpgds*, while ductal cells strongly express the less efficient PGD_2 synthase *Ptgds*. All PGE_2 synthases (*Ptges1–3*) and PGI_2 synthase *Ptgis* are expressed in fibroblasts. The thromboxane (TxA_2, TxB_2) and 12-HHTre synthase *Tbxas1* is detected in macrophages, while 12-HHTre synthase *Cyp2s1* is expressed in PanIN and tumor cells (Figure 2B–C). In terms of lipoxygenase expression, 5-HETE requires co-expression of *Alox5* and its activating protein *Alox5ap*, which are both observed in macrophages, neutrophils, and tuft cells (Figure 2B)[5]. To confirm expression of ALOX5 in tuft cells, we conducted co-immunofluorescence for ALOX5, and COX1 and acetylated-α-tubulin, which label tuft cells in the epithelium. Consistent with studies conducted in the intestines[42], we found that 84% (336/400) of tuft cells (n = 4 *KC* mice) express ALOX5. Conversely, 99.5% (398/400) of ALOX5-expressing cells in the epithelium are tuft cells, suggesting a role for pancreatic tuft cells in 5-HETE synthesis (Figure 2D).

To determine which cell types might respond to relevant eicosanoids, we evaluated patterns of eicosanoid receptor expression. We identified widespread expression of receptor *Pparg* (PGD_2 and PGE_2 metabolites, 15-HETE) in normal and pre-invasive ductal cells as well as in several stromal populations. Expression of PGI_2 receptor *Ptgir* (6k-PGF1α) is concentrated in fibroblasts and pericytes and the thromboxane receptor *Tbxa2r* (TxB_2) is highly expressed in fibroblasts, pericytes, and endothelial cells. PGE_2 receptors were also detected in our analysis, with *Ptger3* expression largely relegated to fibroblasts and *Ptger4* mainly expressed in normal and pre-invasive ductal cells, macrophages, T cells, and fibroblasts (Figure 2 B, E).

Collectively, our eicosanoid profiling and analysis of the Schlesinger et al. scRNA-seq dataset suggest potentially critical cellular sources of key eicosanoids in pre-invasive PanIN. For example, high levels of PGD_2, PGI_2 metabolites (6k-PGF1α), and TxA_2 metabolites (TxB_2) by mass spectrometry may be explained by the expression of requisite synthases in tuft cells and macrophages, fibroblasts, and macrophages, respectively (Figure 2B–C, 2F).

Expression of eicosanoid synthases and receptors in murine models of PDAC

To examine eicosanoid synthase and receptor expression in murine PDAC, we reanalyzed a scRNA-seq dataset generated from *KPC* mice (Figure 3A)[41]. This dataset is comprised of 11,222 cells and libraries were combined and clusters annotated by expression of known cell type markers (Figure S1C). In contrast to the Schlesinger dataset, epithelial clusters in this dataset are largely comprised of tumor cells (Figure 3A). In terms of eicosanoid synthases, we identified expression of phospholipase *Pla2g4a* in tumor cells, fibroblasts, and myeloid cells, with minor expression in neutrophils (Figure 3B). Cyclooxygenases (*Ptgs1*, *Ptgs2*) are expressed primarily in EMT-like tumor cells, myeloid cells, neutrophils, and fibroblasts (Figure 3B). We identified the full complement of genes required to produce PGD_2 (*Hpgds*), thromboxane pathway products TxB_2 and 12-HHTre (*Tbxas1*), and 5-HETE (*Alox5*, *Alox5ap*), as well as *Alox15* (15-HETE, 14- and 17-HdoHE) in myeloid cells. Tumor cells express genes required to produce PGE_2 (*Ptges*) and 12-HHTre (*Cyp2s1*). Although few fibroblasts were profiled in this dataset, enzymes required to produce PGE_2 and PGI_2 (*Ptgis*) were detected. Finally, neutrophils express enzymes required for 5-HETE synthesis (*Alox5*, *Alox5ap*) (Figure 3B–C).

We next examined expression of known eicosanoid receptors. *Pparg*, which mediates the effects of several eicosanoids, is most highly expressed in tumor cells and myeloid cells[5]. PGE_2 receptors are both *Pparg* and thromboxane receptor *Tbxa2r*, consistent with the Schlesinger dataset (Figure 3B–C). To collectively validate our findings in the PanIN and PDAC datasets, we reanalyzed a third scRNA-seq dataset that encompasses normal pancreas, pre-invasive disease, and PDAC in multiple murine models (Figure S2)[43]. Several patterns found in the Schlesinger dataset were identified here as well, notably the presence of *Ptgds* and absence of *Ptges* in the epithelium in early stages of disease progression. Analyses of PDAC are largely in agreement with observations made from the Elyada et. al. dataset, including expression of PGE_2 synthases in tumor cells, *Ptgis* in fibroblasts, and *Tbxas1* in macrophages/myeloid cells (Figure S2).

Cancer-associated fibroblasts (CAFs) have been established as important players in cancer formation and progression and several sub-sets have been identified in PDAC[41, 44]. To determine if eicosanoid synthases and/or receptors are differentially expressed in various CAF sub-types, we re-examined a second scRNA-seq dataset from Elyada et al., consisting of FACS-enriched fibroblasts. This dataset is composed of 8,438 cells generated from four tumor-bearing *KPC* mice and includes three CAF sub-types (iCAFs, myCAFs, apCAFs), perivascular cells, and EpCAM-negative EMT-like tumor cells, as annotated by the original authors (Figure 3D, S1D). We found eicosanoid synthase and receptor expression in this fibroblast-enriched dataset to be largely consistent with our previous analyses, showing that fibroblasts express *Pla2g4a*, *Ptgs1* (COX1), PGE_2 synthases and *Ptgis*. Fibroblasts specifically express PGE_2 receptor *Ptger3*, which is highest in apCAFs. Interestingly, the PGI_2 (6k-PGF1α) receptor, *Ptgir*, is also enriched in perivascular cells suggesting a possible signaling loop between CAFs and perivascular cells (Figure 3E–F).

To evaluate whether orthotopic tumor models recapitulate the patterns of eicosanoid synthase expression we identified in *KPC* mice, we generated tumors using the FC-1199 and FC-1245 PDAC cell lines. Tumors were collected and epithelial (EpCAM+CD45-) or inflammatory (EpCAM-CD45+) cells were isolated by FACS. Separately, RNA was collected from chunks of whole tumor or cell lines grown in 2-D. We then compared expression of eicosanoid synthases between these different models and tissue compartments by qRT-PCR and immunofluorescence. In tumors derived from both cell lines, we found eicosanoid synthases (*Ptgs1*, *Ptgs2*, *Hpgds*, *Alox5*) to be more highly expressed in immune cells than in tumor cells, though expression is not exclusive (Figure S3A–B). PGD_2 synthase *Ptgds* and PGE_2 synthases *Ptges1–3* are also expressed in tumor cells (Figure S3A–B). Fibroblasts are less abundant in these tumors than in autochthonous models, but we were able to identify expression of PTGIS in αSMA+ fibroblasts by immunofluorescence (Figure S3C). Notably, and in comparison, to autochthonous models and human disease (Figures 6–7), eicosanoid synthesis in orthotopic models is dominated by the stromal compartment rather than the tumor cells (Figure S3).

Eicosanoid profiling of human PDAC

To determine if the eicosanoid profiles we generated from murine PDAC are representative of the human condition, we next conducted mass spectrometry on surgical specimens

collected from 12 patients with PDAC, as well as 13 pancreas samples pathologically determined to be normal (Figure 4A, File S1). Eicosanoid profiling of human samples revealed large, significant upregulation of prostaglandins in the thromboxane pathway (TxB_2, 12-HHTre) and the prostacyclin pathway (6k-PGF1α), consistent with observations made in mouse models (Figure 1). Though it did not reach significance, we did see a trend towards increased PGE_2 levels in PDAC (p=0.059), in agreement with previous studies (Figure 4D)[7]. Consistent with our observations in murine orthotopic tumor models, we observed a significant decrease in multiple linoleic acid metabolites in PDAC as compared to normal pancreas (Figure 4B–D). We also detected a significant decrease in free adrenic acid and docosahexaenoic acid (Figure 4D). Interestingly, and in agreement with our previous studies of HPGDS expression, we did not detect high levels of PGD_2 (Figure 4D)[4]. While this may be representative of human PDAC, we cannot exclude confounding factors, such as sample preparation. The lack of detection of additional eicosanoids found to be elevated in mouse models may be due, in part, to degradation.

Eicosanoid gene expression changes during the transition from pre-invasive PanIN to PDAC.

As our eicosanoid profiling analysis of human PDAC identified several species that are also upregulated in mouse models, we next asked whether the cellular sources of these relevant eicosanoid synthases are the same and if they change during the PanIN to PDAC transition. To answer these questions, we examined a bulk RNA sequencing dataset of laser capture microdissected samples of human epithelium and stroma from 26 patients with PanIN and 197 patients with PDAC (124 matched stromal samples, generated as described in[45]). First, we examined cyclooxygenase gene expression patterns. We found that while *PTGS1* (COX1) expression is higher in the stroma than the epithelium in both PanIN and PDAC, there is a significant decrease in gene expression in the epithelium from PanIN to PDAC, consistent with tuft cell loss (Figure 5A)[2]. Interestingly, there is a gain in *PTGS2* (COX2) expression in the epithelium in the transition to PDAC and levels are higher than in the stoma, consistent with a role for tumor cell-derived COX2 (Figure 5A).

Next, we examined expression patterns of terminal prostaglandin synthases. While both PGD_2 synthase *HPGDS* and PGE_2 synthase *PTGES* are expressed in the stroma of PanIN and PDAC, we found a large, significant decrease in *HPGDS* and a gain of *PTGES* expression in the PDAC epithelium (Figure 5A–C). These results suggest a possible switch between tumor suppressive PGD_2 and pro-tumorigenic PGE_2 during the transition from PanIN to PDAC.

Other features of human PDAC identified in this analysis are consistent with what we found in mouse models, namely higher expression of *PTGIS* in the stroma and *CYP2S1* in the epithelium (Figure 5A). Thromboxane synthase *TXBAS1* was detected at comparable levels in the epithelium of both PanIN and PDAC, but is significantly higher in the PDAC stroma, consistent with the increase in TxB_2 levels we found between PanIN and PDAC in mouse models (Figure 5A). While *ALOX5* is expressed at comparable levels in all conditions, *ALOX5AP* is elevated only in stromal samples (Figure 5A). Taken together, these data show that the cell type-specific expression patterns of eicosanoid synthases in human PanIN and

PDAC largely agree with that in mouse models, though tumor cells may play a larger role in human disease (Figure 5B, S4). Over the course of pancreatic tumorigenesis, we observed a shift in the epithelium from *PTGS1*/*HPGDS* to *PTGS2*/*PTGES* expression (Figure 5C). This is consistent with our observation that *PTGS1*+*HPGDS*+ tuft cells are lost in the transition from pre-invasive disease to PDAC[2].

Cell type-specific expression of eicosanoid synthases and receptors in human PDAC

To identify the specific epithelial and stromal cell types that express relevant eicosanoid synthases and receptors in human PDAC, we next examined a scRNA-seq dataset of 11 normal pancreata and 24 PDAC samples including 57,530 cells[46]. We first subsetted the tumor samples (41,986 cells) and identified cell types by markers described in Peng et al. (Figure 6A). Interestingly, we identified a large degree of heterogeneity in synthase expression among malignant tumor cells, possibly reflecting the inter-tumor heterogeneity of patients included in this study (Figure 6B–C). Within the tumor population, we identified expression of phospholipase enzymes *PLA2G2A* and *PLA2G4A* and *PTGS2* (COX2), but not *PTGS1* (COX1) (Fig 6B–C). Tumor cells express synthases *TBXAS1* (TXA_2, TXB_2, 12-HHTre) and *CYP2S1* (12-HHTre) and some subclusters are enriched for PGE_2 synthase *PTGES* or prostacyclin synthase *PTGIS* (Figure 6B–C). A small subset of 49 cells that cluster with ductal cells are tuft cells and express both *PTGS1* and *HPGDS*, as previously described (Figure S5A)[2]. In terms of the stroma, we identified expression of *PTGS1*, *TBXAS1*, and *CYP2S1* enriched in macrophages. A subset of these cells also weakly express *HPGDS*. PDAC CAFs express *PTGDS* (PGD_2), *PTGES* (PGE_2), and *PTGIS* (PGI_2) (Figure 6B–C). *ALOX5/ALOX5AP* (5-HETE) co-expression is largely detected in myeloid cells, but also in B cells. Consistent with the Maurer dataset, *ALOX15B* (15-HETE, 17-HdoHE) is expressed in myeloid cells and fibroblasts (Figure 6B, S4)[45]. To confirm these data, we interrogated a second scRNA-seq dataset of human PDAC containing 8000 cells and 10 patients[47]. As shown in Figure S5B, we found that eicosanoid synthase expression patterns in these two datasets are largely in agreement[46].

To infer what cell types might respond to eicosanoids in the PDAC microenvironment, we next examined expression of relevant receptors. *PPARG* (PGD_2 and PGE_2 metabolites, 15-HETE) expression is widespread and can be found in tumor cells, myeloid cells, stellate cells, and endothelial cells, with minor expression in several other cell types. *PTGER2* and *PTGER4* share similar patterns of expression, highest in myeloid cells, T cells, and fibroblasts, while *PTGER3* is specifically expressed in stellate cells and fibroblasts. PGD_2 receptor *PTGDR* is expressed in T cells, fibroblasts, and stellate cells. As seen in murine models, *PTGIR* (PGI_2, 6k-PGF1α) is highly expressed in stellate cells and fibroblasts and *TBXA2R* (TxB_2, TxA_2) is most highly expressed in endothelial cells (Figure 6D).

To reconcile inferences made from the RNA-seq studies with eicosanoids detected by mass spectrometry, we conducted immunostaining for PTGIS, PTGES, and TBXAS1 in several tissue samples spanning normal pancreas, PanIN, and PDAC. Consistent with sequencing studies, we identified expression of PTGIS and PTGES in both αSMA+ fibroblasts and in tumor cells. TBXAS1 is expressed in both CD68+ macrophages and the tumor epithelium (Figure 6F–G).

To take a more quantitative approach, we next conducted immunohistochemistry (IHC) and scored expression of these synthases in multiple tissue compartments of samples from 22 treatment naïve PDAC patients. By sampling multiple surgical samples from the same patients, our analysis spanned normal tissue, metaplasia, high and low grade PanIN, well and poorly differentiated PDAC, and myxoid or compact stroma totaling 1176 regions of interest (Figure 7A, File S2). We note several observations from these analyses, including a significant increase in PTGES expression in the epithelium with disease progression, as predicted in Figure 5, highest in poorly differentiated PDAC. We also identified a significant increase in PTGIS in the stroma and in TBXAS1 in the epithelium of high grade PanIN, as compared to normal tissue, (Figure 7A–B). Using the same data, Spearman Rho correlation analyses between all the datapoint classes identify significant positive and inverse correlations mostly in interrogated normal duct areas (Figure S6A). Notably, PTGIS, PTGES, and TBXAS1 show positively correlated expression in both epithelial and stromal components ($p=0.005–0.003\times10^{-5}$), while PTGIS and TBXAS1 have an inverse correlation in normal duct epithelium (p=0.004). Furthermore, the stroma underlying poorly differentiated PDAC showed an inverse relationship between PTGIS and PTGES (p=0.032).

Finally, to determine if synthase expression correlates to patient survival, we interrogated the TCGA database (150 PDAC patients) as well as the laser-captured RNA-seq dataset (Maurer et al., manuscript in preparation, 197 PDAC epithelium, 124 PDAC stroma samples) described in Figure 5. As shown in Figure 7, we identified a survival advantage for patients with low PTGES expression in both datasets, and for patients with low PTGIS expression in the Maurer dataset (Figure 7C–D). Interestingly, it is tumor cell, and not stromal, expression of PTGES that is associated with a survival advantage in the Maurer dataset (Figure 7D–E, S5B). This may reflect different functions for fibroblast vs. tumor cell derived PGE_2 in PDAC. Collectively, these data suggest that tumor cell expression of eicosanoid synthases is associated with pathogenesis and reduced patient survival.

Discussion

In this study, we conducted eicosanoid profiling on normal pancreata and PDAC in mouse models of pancreatic tumorigenesis and patient samples, interrogated published RNA-seq datasets to generate predictions as to the cellular origin of eicosanoid species, and validated key findings at the protein level. The data collectively suggest a previously undescribed role for prostacyclin and thromboxane signaling in pancreatic tumorigenesis. Both prostacyclins and thromboxanes have known roles in blood clotting. The incidence of thrombosis is particularly high in patients with PDAC (up to 57%) and thromboembolic diseases are the second most common cause for mortality, accounting for 44% of total deaths after cancer progression[48, 49]. These data indicate that targeting prostacyclin or thromboxane signaling pathways in PDAC may have the added benefit of inhibiting thrombotic events.

Transcriptomic data from both human and mouse samples suggest an “eicosanoid switch” in the epithelium, from PGD_2-producing enzymes in PanIN to PGE_2-producing enzymes in PDAC. Our analysis of the human condition suggests that this gain in synthase expression in tumor cells is associated with reduced survival. In mouse models, the stroma appears to be the dominant source of eicosanoid synthesis, a potentially critical difference between mouse

models and human disease. These analyses provide a valuable resource for further functional investigation.

We note certain limitations in the conclusions drawn from the analytical techniques we have used. Although eicosanoid profiling by mass spectrometry informed us of targets highly upregulated in PDAC, the detection of these species may have been impacted by their half-lives. For example, while it can be hypothesized that the relative lack of diversity in eicosanoid species in human PDAC may be a result of years-long immune reprogramming to an immunosuppressed state, in contrast to the months-long time course of tumor progression in mouse models, an equally viable hypothesis is that this lack of eicosanoid diversity is merely a technical artifact arising from sample processing post-surgery. This differs from the relatively quick preservation of mouse tumor samples. In support of the latter hypothesis is the fact that the three significantly upregulated eicosanoids – or their metabolites – in human tumors have relatively long half-lives. However, the trend towards higher PGE_2 levels, which has a half-life of only 2.5–5 minutes may serve as a positive control[50]. These hypotheses may be resolved by accurate *in situ* studies aimed at identifying synthase functionality.

RNA sequencing based analyses also present key limitations. RNA expression does not always correlate with protein expression or activity, the latter of which is largely dependent on post-transcriptional factors, post-translational factors, enzyme localization and substrate availability, and signaling cues. Secondly, the scRNA-seq datasets we used to localize eicosanoid synthase/receptor expression are unsuitable to study platelets, whose small size and lack of a nucleus excluded them from collection. Platelets synthesize eicosanoids (PGE_2, PGD_2, 11-HETE, 15-HETE, and others) in various contexts, such as wound healing, and tumor infiltrating platelets have been described in pancreatic neuroendocrine tumors[51, 52]. Activated platelets could represent a major source of eicosanoid diversity uncharacterized by our analyses.

Despite these limitations, our analyses identify eicosanoids that warrant further investigation in the context of pancreatic tumorigenesis. Our multifaceted approach enabled us to make novel predictions regarding patterns of eicosanoid synthesis in PanIN and PDAC. We have confirmed these predictions at the synthase RNA, synthase protein, and eicosanoid levels. Notably, many patterns of eicosanoid synthase expression identified in this study are consistent with previous studies in PDAC or in other organ systems. Collectively, our work localizes eicosanoid synthases to specific cell types in PDAC and underscores the need to determine the function of these species in pancreatic cancer development and progression. Understanding the role of various eicosanoids in PDAC may identify pathways to co-opt or novel targets for treatment.

Supplementary Material

Refer to Web version on PubMed Central for supplementary material.

Acknowledgements:

The authors thank Taylor Culpepper for technical assistance and Amy Cao for artistic rendering and illustrator services. Tissue samples were provided by the NCI Cooperative Human Tissue Network (CHTN). Other investigators may have received specimens from the same tissue specimens.

Funding:

N.K.L. was supported by the Salk Institute Cancer Training Grant T32 CA009370, a Hope Funds for Cancer Research Postdoctoral Fellowship (HFCR-20-03-03), and a Sky Foundation Seed Grant. S.Z. was supported by NIH/NCI K00CA222741. The Flow Cytometry Core Facility at the Salk Institute is funded by NIH/NCI P30 CA014195 and Shared Instrumentation Grant S10-OD023. P.K.S. is supported by funding from the NIH/NCI (R01CA210439, R01CA163649, R01CA216853, NCI) and the Fred & Pamela Buffett Cancer Center Support Grant (P30CA036727). Work in the Olive laboratory is supported by the Herbert Irving Comprehensive Cancer Center Support Grant (P30CA013696) and the Pancreas Center of New York Presbyterian Hospital. M.C.B.T is supported by a Vanderbilt Digestive Disease Research Center Pilot and Feasibility Grant (P30 DK058404) and a Nikki Mitchell Foundation Pancreas Club Seed Grant. The Hunter laboratory was supported by NIH/NCI CA082683 and a Lustgarten Foundation Award (#552873). T.H. is a Frank and Else Schilling American Cancer Society Professor and the Renato Dulbecco Chair in Cancer Research. The Kaech laboratory was supported by NIH/NCI 5R01 CA240909-02. Work in the Wahl laboratory is supported, in part, by the Salk Institute Cancer Center Core Grant (CA014195), NIH-NCI R35 CA197687, NIH-NCI T32 CA009370, NIH/NCI 5R01 CA240909-02, the Isacoff Gastrointestinal Research Foundation, the Freeberg Foundation, and the Leona M. and the Harry B. Helmsley Charitable Trust (2012-PG-MED002). The DelGiorno laboratory is supported by NIH/NCI 5R01 CA240909-02, the Vanderbilt-Ingram Cancer Center Support Grant (P30 CA068485), a Vanderbilt Digestive Disease Research Center Pilot and Feasibility Grant (P30 058404), an American Gastroenterological Association Research Scholar Award (AGA2021-13-02), NIH/NIGMS GM142709, The Sky Foundation, Inc. (AWD00000079), and Linda's Hope (Nashville, TN).

References

1. Storz P Acinar cell plasticity and development of pancreatic ductal adenocarcinoma. Nat Rev Gastroenterol Hepatol 2017;14:296–304. [PubMed: 28270694]
2. Delgiorno KE, Hall JC, Takeuchi KK, et al. Identification and manipulation of biliary metaplasia in pancreatic tumors. Gastroenterology 2014;146:233–44 e5. [PubMed: 23999170]
3. DelGiorno KE, Naeem RF, Fang L, et al. Tuft Cell Formation Reflects Epithelial Plasticity in Pancreatic Injury: Implications for Modeling Human Pancreatitis. Front Physiol 2020;11:88. [PubMed: 32116793]
4. DelGiorno KE, Chung CY, Vavinskaya V, et al. Tuft Cells Inhibit Pancreatic Tumorigenesis in Mice by Producing Prostaglandin D2. Gastroenterology 2020.
5. Wang D, Dubois RN. Eicosanoids and cancer. Nat Rev Cancer 2010;10:181–93. [PubMed: 20168319]
6. Bui P, Imaizumi S, Beedanagari SR, et al. Human CYP2S1 metabolizes cyclooxygenase- and lipoxygenase-derived eicosanoids. Drug Metab Dispos 2011;39:180–90. [PubMed: 21068195]
7. Markosyan N, Li J, Sun YH, et al. Tumor cell-intrinsic EPHA2 suppresses anti-tumor immunity by regulating PTGS2 (COX-2). J Clin Invest 2019;129:3594–3609. [PubMed: 31162144]
8. Wang D, Cabalag CS, Clemons NJ, et al. Cyclooxygenases and Prostaglandins in Tumor Immunology and Microenvironment of Gastrointestinal Cancer. Gastroenterology 2021.
9. Yan M, Myung SJ, Fink SP, et al. 15-Hydroxyprostaglandin dehydrogenase inactivation as a mechanism of resistance to celecoxib chemoprevention of colon tumors. Proc Natl Acad Sci U S A 2009;106:9409–13. [PubMed: 19470469]
10. Arima K, Ohmuraya M, Miyake K, et al. Inhibition of 15-PGDH causes Kras-driven tumor expansion through prostaglandin E2-ALDH1 signaling in the pancreas. Oncogene 2019;38:1211–1224. [PubMed: 30250298]
11. Zhang B, Bie Q, Wu P, et al. PGD2/PTGDR2 Signaling Restricts the Self-Renewal and Tumorigenesis of Gastric Cancer. Stem Cells 2018;36:990–1003. [PubMed: 29604141]
12. Tippin BL, Kwong AM, Inadomi MJ, et al. Intestinal tumor suppression in ApcMin/+ mice by prostaglandin D2 receptor PTGDR. Cancer Med 2014;3:1041–51. [PubMed: 24729479]

13. Li H, Lee MH, Liu K, et al. Inhibiting breast cancer by targeting the thromboxane A2 pathway. NPJ Precis Oncol 2017;1:8. [PubMed: 29872696]
14. Lucotti S, Cerutti C, Soyer M, et al. Aspirin blocks formation of metastatic intravascular niches by inhibiting platelet-derived COX-1/thromboxane A2. J Clin Invest 2019;129:1845–1862. [PubMed: 30907747]
15. Ekambaram P, Lambiv W, Cazzolli R, et al. The thromboxane synthase and receptor signaling pathway in cancer: an emerging paradigm in cancer progression and metastasis. Cancer Metastasis Rev 2011;30:397–408. [PubMed: 22037941]
16. Roberts LJ 2nd, Sweetman BJ, Payne NA, et al. Metabolism of thromboxane B2 in man. Identification of the major urinary metabolite. J Biol Chem 1977;252:7415–7. [PubMed: 914816]
17. Liu M, Saeki K, Matsunobu T, et al. 12-Hydroxyheptadecatrienoic acid promotes epidermal wound healing by accelerating keratinocyte migration via the BLT2 receptor. J Exp Med 2014;211:1063–78. [PubMed: 24821912]
18. Okuno T, Yokomizo T. Biological functions of 12(S)-hydroxyheptadecatrienoic acid as a ligand of leukotriene B4 receptor 2. Inflamm Regen 2018;38:29. [PubMed: 30397418]
19. Osawa T, Ohga N, Hida Y, et al. Prostacyclin receptor in tumor endothelial cells promotes angiogenesis in an autocrine manner. Cancer Sci 2012;103:1038–44. [PubMed: 22380928]
20. Dai D, Chen B, Feng Y, et al. Prognostic value of prostaglandin I2 synthase and its correlation with tumor-infiltrating immune cells in lung cancer, ovarian cancer, and gastric cancer. Aging (Albany NY) 2020;12:9658–9685. [PubMed: 32463792]
21. Moncada S, Gryglewski R, Bunting S, et al. An enzyme isolated from arteries transforms prostaglandin endoperoxides to an unstable substance that inhibits platelet aggregation. Nature 1976;263:663–5. [PubMed: 802670]
22. Snodgrass RG, Brune B. Regulation and Functions of 15-Lipoxygenases in Human Macrophages. Front Pharmacol 2019;10:719. [PubMed: 31333453]
23. Conteh AM, Reissaus CA, Hernandez-Perez M, et al. Platelet-type 12-lipoxygenase deletion provokes a compensatory 12/15-lipoxygenase increase that exacerbates oxidative stress in mouse islet beta cells. J Biol Chem 2019;294:6612–6620. [PubMed: 30792307]
24. Mozurkewich EL, Greenwood M, Clinton C, et al. Pathway Markers for Pro-resolving Lipid Mediators in Maternal and Umbilical Cord Blood: A Secondary Analysis of the Mothers, Omega-3, and Mental Health Study. Front Pharmacol 2016;7:274. [PubMed: 27656142]
25. Austin Pickens C, Yin Z, Sordillo LM, et al. Arachidonic acid-derived hydroxyeicosatetraenoic acids are positively associated with colon polyps in adult males: a cross-sectional study. Sci Rep 2019;9:12033.
26. Ghosh J, Myers CE. Inhibition of arachidonate 5-lipoxygenase triggers massive apoptosis in human prostate cancer cells. Proc Natl Acad Sci U S A 1998;95:13182–7. [PubMed: 9789062]
27. Avis I, Hong SH, Martinez A, et al. Five-lipoxygenase inhibitors can mediate apoptosis in human breast cancer cell lines through complex eicosanoid interactions. FASEB J 2001;15:2007–9. [PubMed: 11511519]
28. O'Flaherty JT, Wooten RE, Samuel MP, et al. Fatty acid metabolites in rapidly proliferating breast cancer. PLoS One 2013;8:e63076.
29. Shappell SB, Gupta RA, Manning S, et al. 15S-Hydroxyeicosatetraenoic acid activates peroxisome proliferator-activated receptor gamma and inhibits proliferation in PC3 prostate carcinoma cells. Cancer Res 2001;61:497–503. [PubMed: 11212240]
30. Zhang Q, Zhu B, Li Y. Resolution of Cancer-Promoting Inflammation: A New Approach for Anticancer Therapy. Front Immunol 2017;8:71. [PubMed: 28210259]
31. Valdes AM, Ravipati S, Menni C, et al. Association of the resolvin precursor 17-HDHA, but not D- or E-series resolvins, with heat pain sensitivity and osteoarthritis pain in humans. Sci Rep 2017;7:10748.
32. Sulciner ML, Serhan CN, Gilligan MM, et al. Resolvins suppress tumor growth and enhance cancer therapy. J Exp Med 2018;215:115–140. [PubMed: 29191914]
33. Zhang Y, Kirane A, Huang H, et al. Cyclooxygenase-2 Inhibition Potentiates the Efficacy of Vascular Endothelial Growth Factor Blockade and Promotes an Immune Stimulatory

Microenvironment in Preclinical Models of Pancreatic Cancer. Mol Cancer Res 2019;17:348–355. [PubMed: 30333153]

34. Kirane A, Toombs JE, Ostapoff K, et al. Apricoxib, a novel inhibitor of COX-2, markedly improves standard therapy response in molecularly defined models of pancreatic cancer. Clin Cancer Res 2012;18:5031–42. [PubMed: 22829202]
35. Bardeesy N, Aguirre AJ, Chu GC, et al. Both p16(Ink4a) and the p19(Arf)-p53 pathway constrain progression of pancreatic adenocarcinoma in the mouse. Proc Natl Acad Sci U S A 2006;103:5947–52. [PubMed: 16585505]
36. Hingorani SR, Wang L, Multani AS, et al. Trp53R172H and KrasG12D cooperate to promote chromosomal instability and widely metastatic pancreatic ductal adenocarcinoma in mice. Cancer Cell 2005;7:469–83. [PubMed: 15894267]
37. Quehenberger O, Armando AM, Brown AH, et al. Lipidomics reveals a remarkable diversity of lipids in human plasma. J Lipid Res 2010;51:3299–305. [PubMed: 20671299]
38. Wang Y, Armando AM, Quehenberger O, et al. Comprehensive ultra-performance liquid chromatographic separation and mass spectrometric analysis of eicosanoid metabolites in human samples. J Chromatogr A 2014;1359:60–9. [PubMed: 25074422]
39. Hingorani SR, Petricoin EF, Maitra A, et al. Preinvasive and invasive ductal pancreatic cancer and its early detection in the mouse. Cancer Cell 2003;4:437–50. [PubMed: 14706336]
40. Schlesinger Y, Yosefov-Levi O, Kolodkin-Gal D, et al. Single-cell transcriptomes of pancreatic preinvasive lesions and cancer reveal acinar metaplastic cells' heterogeneity. Nat Commun 2020;11:4516. [PubMed: 32908137]
41. Elyada E, Bolisetty M, Laise P, et al. Cross-Species Single-Cell Analysis of Pancreatic Ductal Adenocarcinoma Reveals Antigen-Presenting Cancer-Associated Fibroblasts. Cancer Discov 2019;9:1102–1123. [PubMed: 31197017]
42. McGinty JW, Ting HA, Billipp TE, et al. Tuft-Cell-Derived Leukotrienes Drive Rapid Anti-helminth Immunity in the Small Intestine but Are Dispensable for Anti-protist Immunity. Immunity 2020;52:528–541 e7. [PubMed: 32160525]
43. Hosein AN, Huang H, Wang Z, et al. Cellular heterogeneity during mouse pancreatic ductal adenocarcinoma progression at single-cell resolution. JCI Insight 2019;5.
44. Biffi G, Oni TE, Spielman B, et al. IL1-Induced JAK/STAT Signaling Is Antagonized by TGFbeta to Shape CAF Heterogeneity in Pancreatic Ductal Adenocarcinoma. Cancer Discov 2019;9:282–301. [PubMed: 30366930]
45. Maurer C, Holmstrom SR, He J, et al. Experimental microdissection enables functional harmonisation of pancreatic cancer subtypes. Gut 2019;68:1034–1043. [PubMed: 30658994]
46. Peng J, Sun BF, Chen CY, et al. Single-cell RNA-seq highlights intra-tumoral heterogeneity and malignant progression in pancreatic ductal adenocarcinoma. Cell Res 2019;29:725–738. [PubMed: 31273297]
47. Lin W, Noel P, Borazanci EH, et al. Single-cell transcriptome analysis of tumor and stromal compartments of pancreatic ductal adenocarcinoma primary tumors and metastatic lesions. Genome Med 2020;12:80. [PubMed: 32988401]
48. Thomas GM, Panicot-Dubois L, Lacroix R, et al. Cancer cell-derived microparticles bearing P-selectin glycoprotein ligand 1 accelerate thrombus formation in vivo. J Exp Med 2009;206:1913–27. [PubMed: 19667060]
49. Blom JW, Osanto S, Rosendaal FR. High risk of venous thrombosis in patients with pancreatic cancer: a cohort study of 202 patients. Eur J Cancer 2006;42:410–4. [PubMed: 16321518]
50. Bygdeman M Pharmacokinetics of prostaglandins. Best Pract Res Clin Obstet Gynaecol 2003;17:707–16. [PubMed: 12972009]
51. Xu SS, Xu HX, Wang WQ, et al. Tumor-infiltrating platelets predict postoperative recurrence and survival in resectable pancreatic neuroendocrine tumor. World J Gastroenterol 2019;25:6248–6257. [PubMed: 31749595]
52. Crescente M, Menke L, Chan MV, et al. Eicosanoids in platelets and the effect of their modulation by aspirin in the cardiovascular system (and beyond). Br J Pharmacol 2019;176:988–999. [PubMed: 29512148]

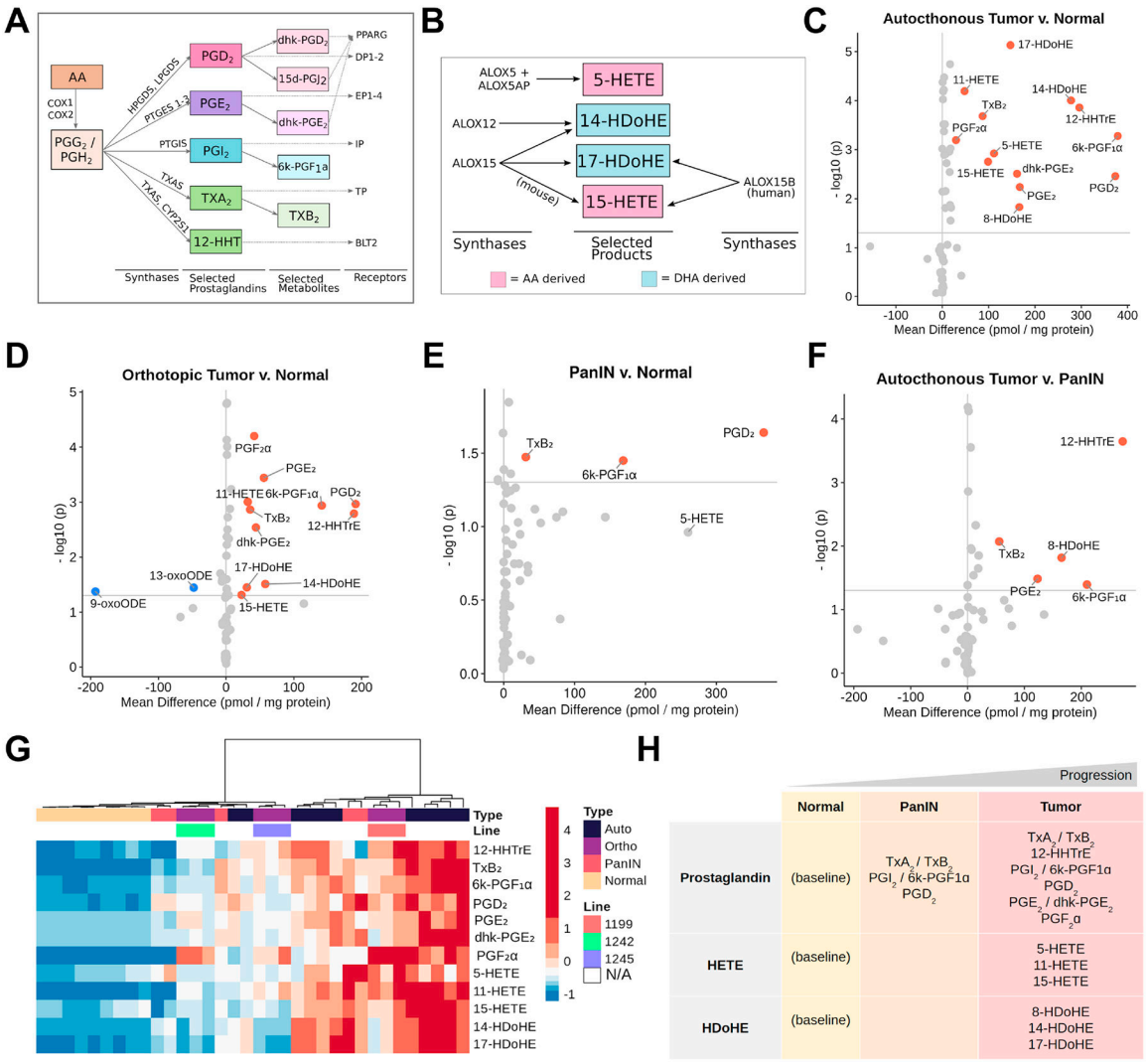

Figure 1. Eicosanoid levels throughout disease progression in mouse models of pancreatic tumorigenesis.

Schematics depicting biosynthesis of select (**A**) prostaglandins and (**B**) HETEs/HDHEs, along with relevant synthases and receptors. Eicosanoid profiles of (**C**) autochthonous tumors (*KPC* mice), (**D**) orthotopic tumors (FC-1199, FC-1242, FC-1245 cell lines), and (**E**) PanIN-bearing pancreata (*KC* mice) with respect to normal pancreas values. (**F**) Eicosanoid levels in autochthonous tumors with respect to PanIN. All values, pmol/mg protein. Samples with a mean difference +/− 20 pmol/mg protein and $p < 0.05$ are indicated in either red, up, or blue, down. (**G**) Hierarchical clustering and heatmap of select eicosanoid levels in the samples shown in C-F. Heatmap values are z-score normalized by row and colors are assigned by quintile scaling. (**H**) Schematic of major eicosanoids associated with pancreatic tumorigenesis in mouse models.

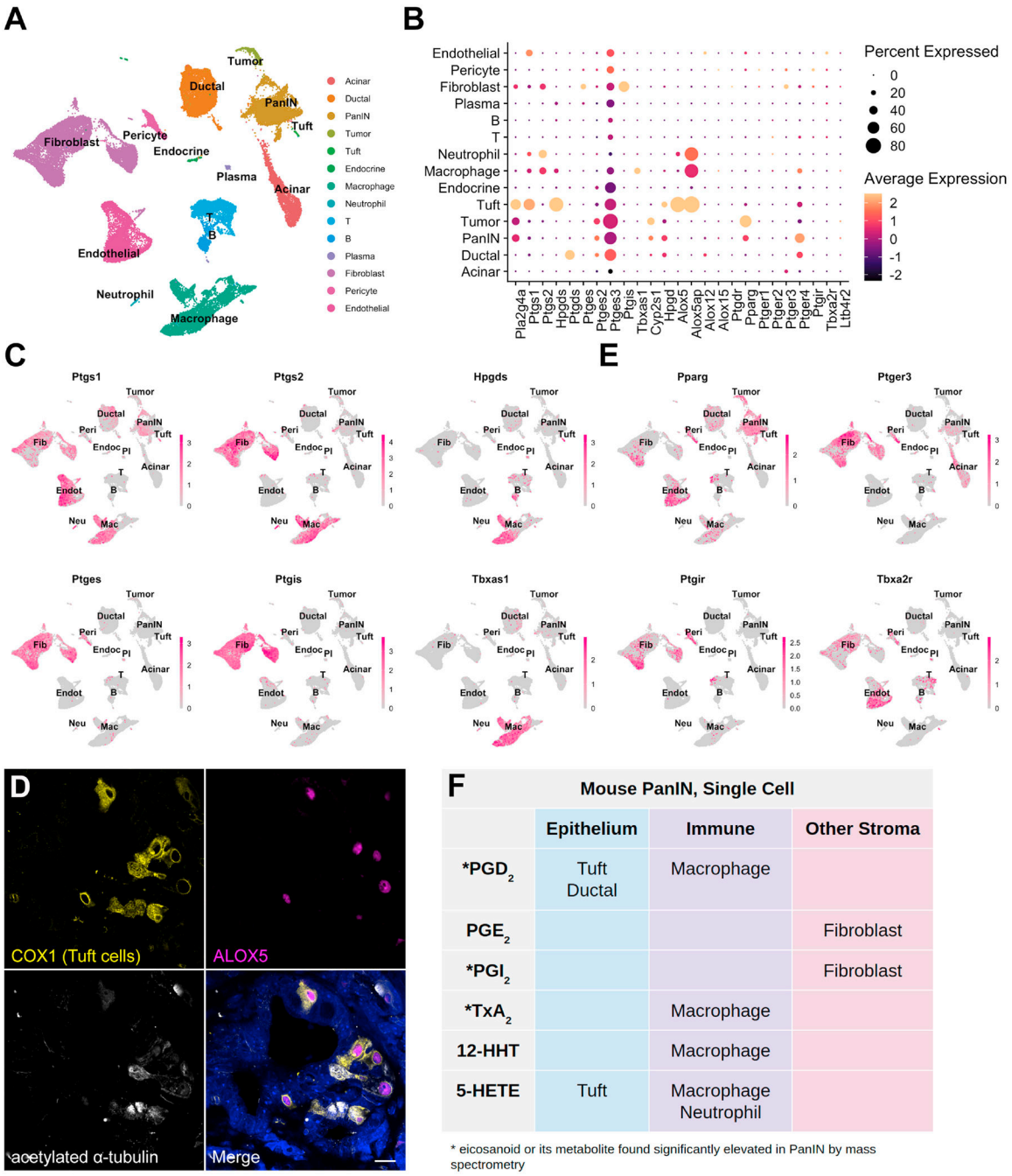

F

Mouse PanIN, Single Cell

	Epithelium	Immune	Other Stroma
***PGD$_2$**	Tuft Ductal	Macrophage	
PGE$_2$			Fibroblast
***PGI$_2$**			Fibroblast
***TxA$_2$**		Macrophage	
12-HHT		Macrophage	
5-HETE	Tuft	Macrophage Neutrophil	

* eicosanoid or its metabolite found significantly elevated in PanIN by mass spectrometry

Figure 2. Cell type-specific expression of eicosanoid synthases and receptors in murine PanIN.

(**A**) UMAP of a murine PanIN scRNA-seq dataset, generated from Schlesinger et al., annotated by cell type. (**B**) Dotplot of average and percent expression of select eicosanoid synthases and receptors in each cell type identified. (**C**) UMAPs depicting gene expression of select eicosanoid synthases. (**D**) Co-IF for COX1 (yellow), ALOX5 (magenta), and acetylated α-tubulin (white) in a *KC* pancreas. DAPI, blue. Scale bar, 10 μm. (**E**) UMAPs depicting gene expression of select eicosanoid receptors. Color intensity in (C) and (E)

indicates the normalized gene expression level for a given gene in each cell. (**F**) Table summarizing inferred cellular sources of eicosanoids based on synthase expression patterns.

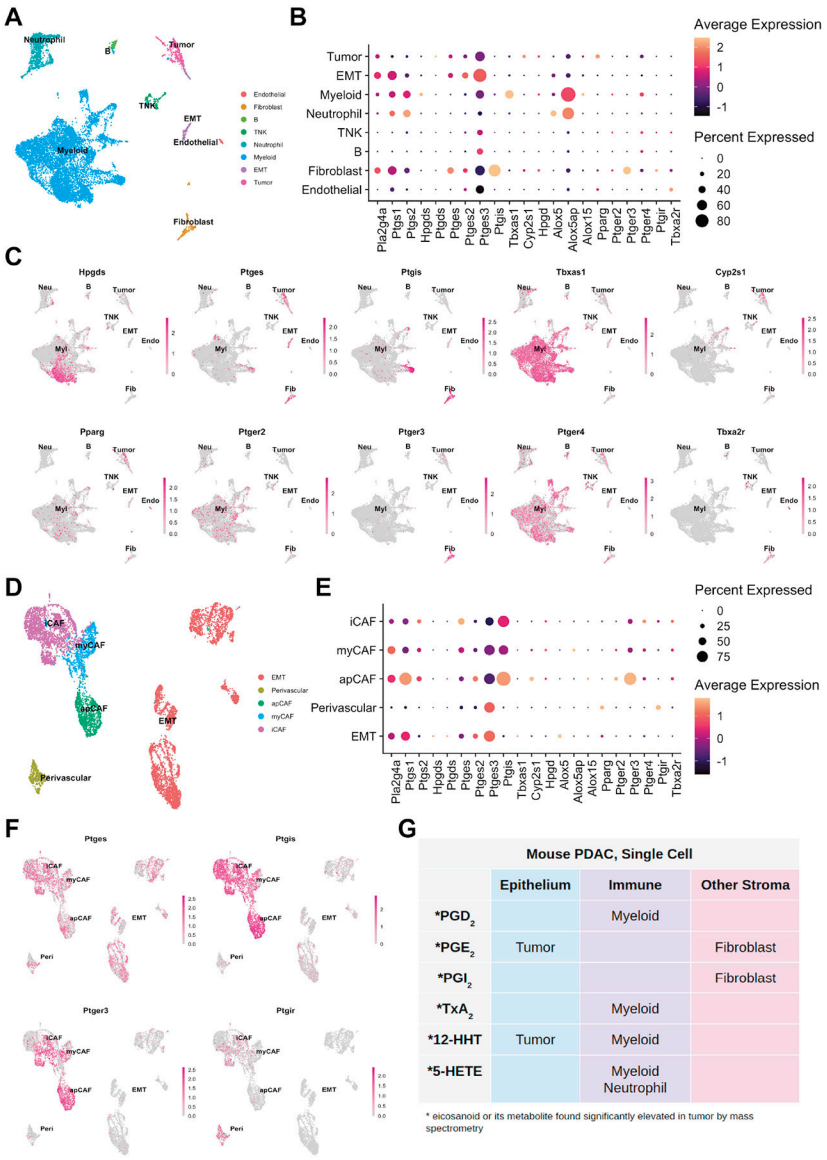

Figure 3. Cell type-specific expression of eicosanoid synthases and receptors in murine models of PDAC.

(**A**) UMAP of a murine PDAC (*KPC*) scRNA-seq dataset derived from Elyada et al., annotated by cell type. EMT, epithelial to mesenchymal transition; TNK, T and natural killer cell. (**B**) Dotplot of average and percent expression of select eicosanoid synthases and receptors in each cell type. (**C**) UMAPs depicting gene expression of select eicosanoid synthases/receptors. (**D**) UMAP of a FACS-enriched CAF dataset derived from Elyada et al., annotated by cell type. iCAF, inflammatory cancer associated fibroblast; myCAF, myofibroblastic CAF; apCAF, antigen presenting CAF. (**E**) Dotplot of average and percent expression of select eicosanoid synthases and receptors in each cell type. (**F**) UMAPs depicting gene expression of select eicosanoid synthases/receptors. Color intensity in (C) and (F) indicates the normalized gene expression level for a given gene in each cell. (**G**) Table summarizing inferred cellular sources of eicosanoids based on patterns of synthase expression.

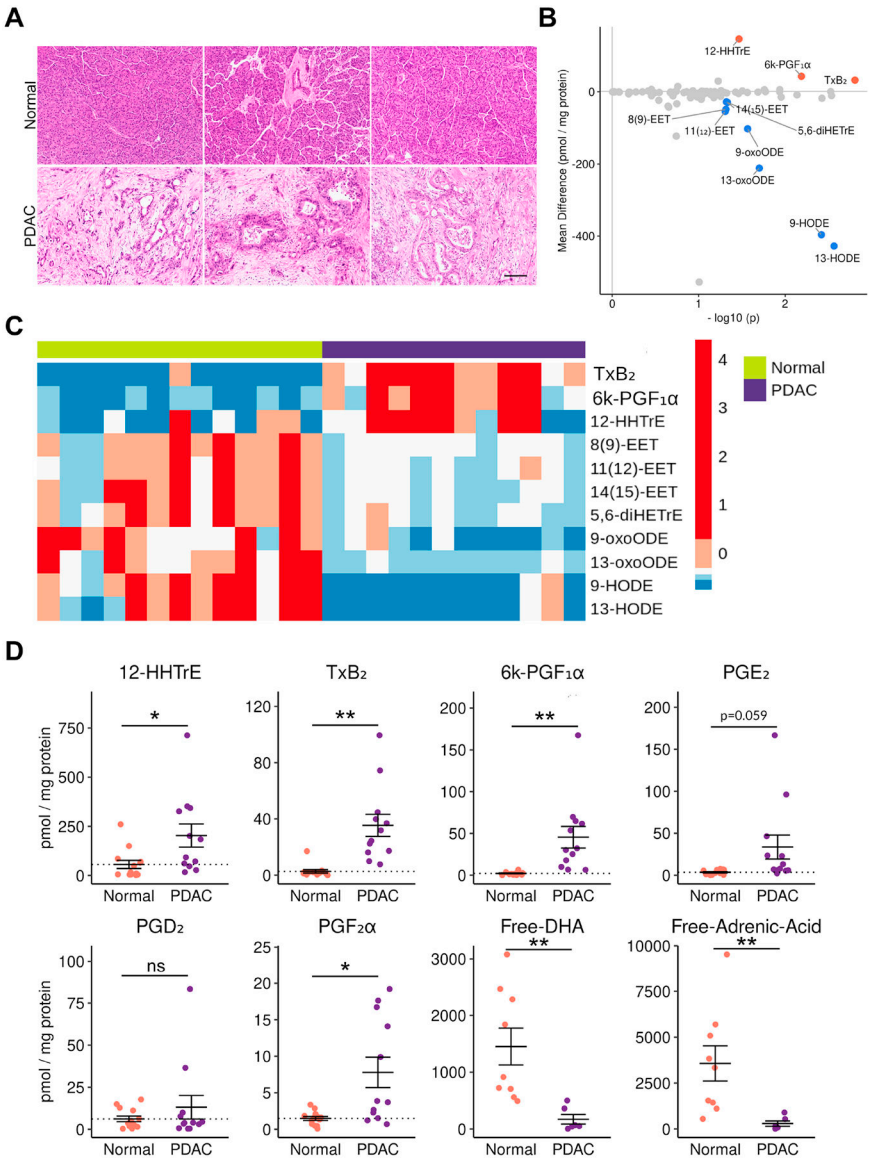

Figure 4. Eicosanoid profiling of human PDAC.

(**A**) Representative H&E of normal human pancreata and PDAC samples. Scale bar, 100 μm. (**B**) Comparison of normal pancreas and PDAC eicosanoid profiles (pmol/mg protein). Samples with a mean difference > +/− 20 pmol/mg protein and $p < 0.05$ are indicated in either red, up, or blue, down. (**C**) Heatmap of select eicosanoids from normal pancreata and PDAC. Values are z-score normalized by row and colors are assigned by quintile scaling. (**D**) Dotplots of select eicosanoids. Error bars, standard error of the mean. *, $p < 0.05$; **, $p < 0.01$; ***, $p < 0.001$; ****, $p < 0.0001$.

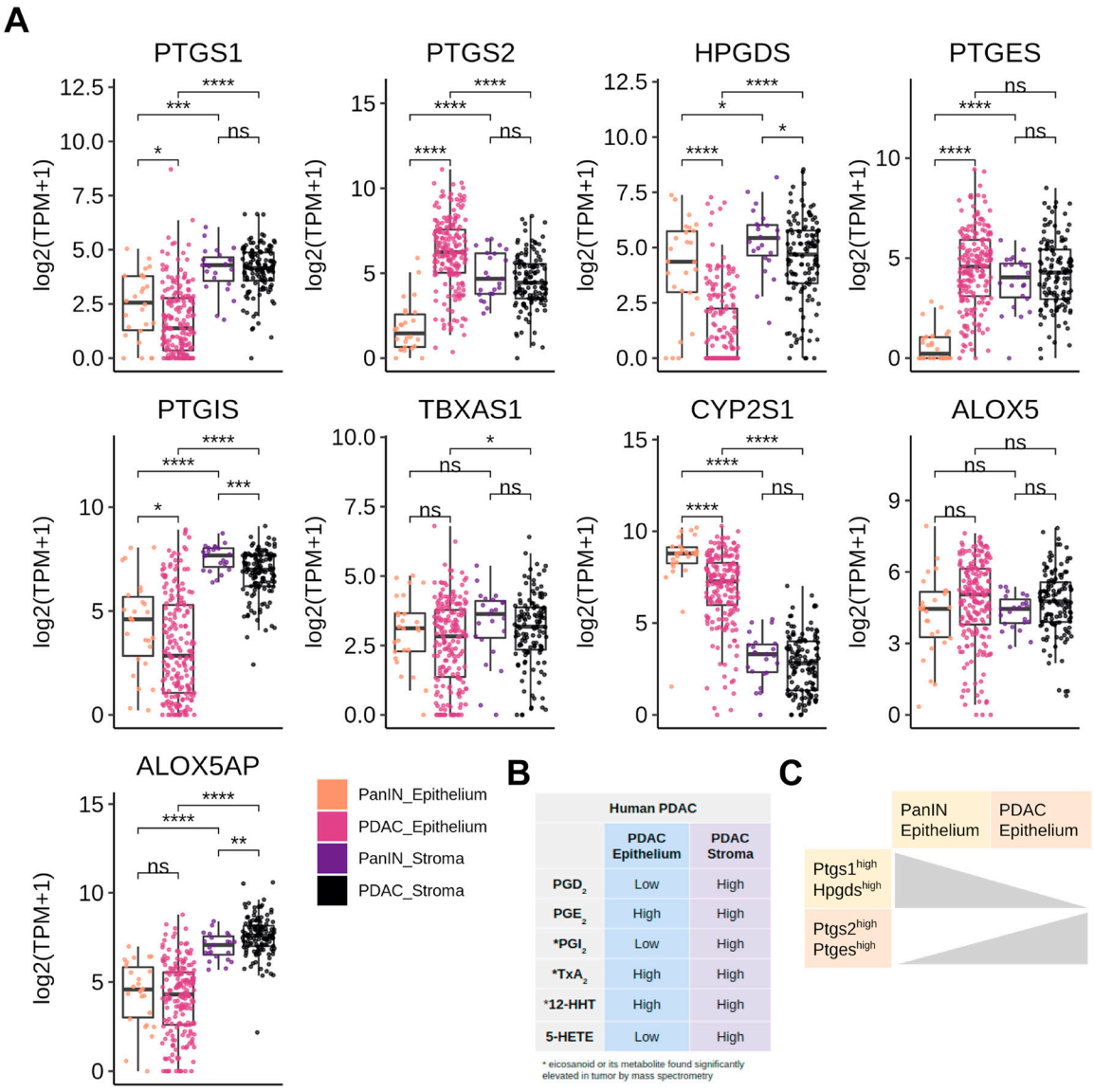

Figure 5. Eicosanoid synthase expression in human PanIN and PDAC.

(**A**) Boxplots comparing expression (log2(TPM+1)) of microdissected stroma and epithelium from PanIN (n = 26) and PDAC (n = 197 epithelium, 124 stroma). *, $p < 0.05$; **, $p < 0.01$; ***, $p < 0.001$; ****, $p < 0.0001$. (**B**) Qualitative summary describing relative localization of terminal eicosanoid synthases in either the tumor epithelium or stroma. (**C**) Summary schematic describing a switch in prostaglandin synthase expression in the epithelium transitioning from PanIN to PDAC.

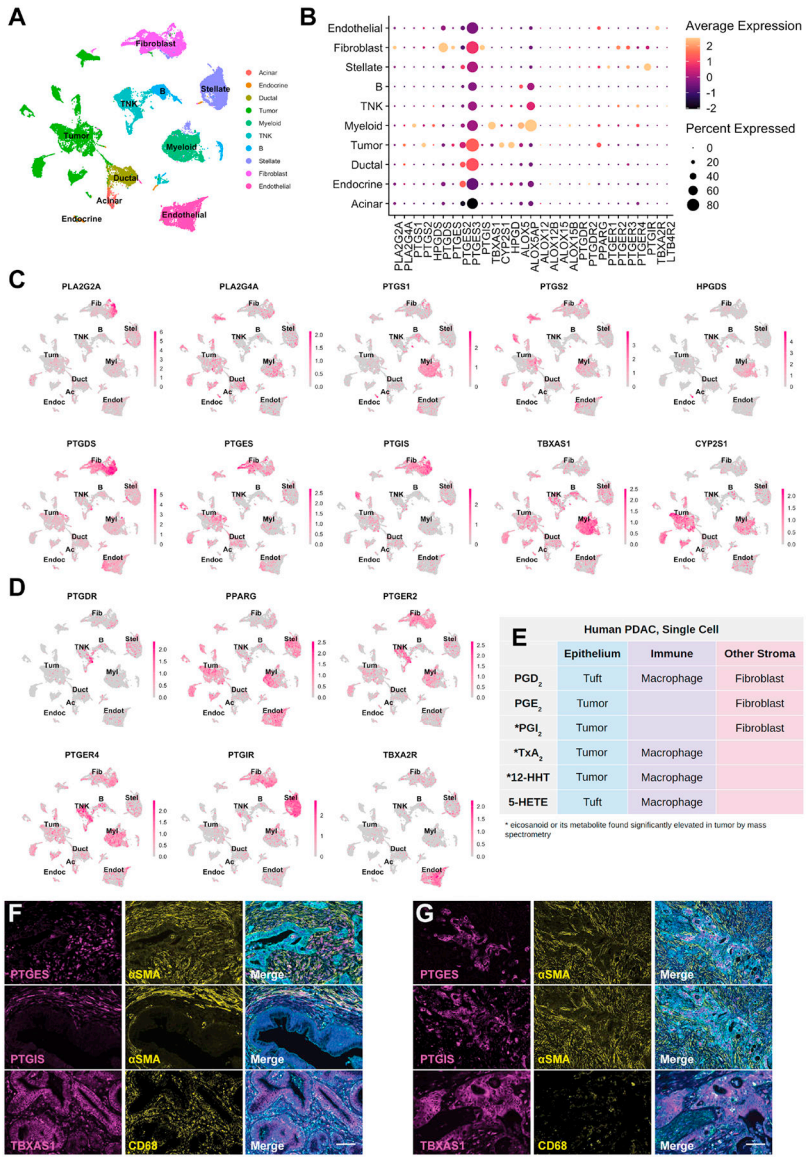

	Epithelium	Immune	Other Stroma
PGD_2	Tuft	Macrophage	Fibroblast
PGE_2	Tumor		Fibroblast
*PGI_2	Tumor		Fibroblast
*TxA_2	Tumor	Macrophage	
*12-HHT	Tumor	Macrophage	
5-HETE	Tuft	Macrophage	

* eicosanoid or its metabolite found significantly elevated in tumor by mass spectrometry

Figure 6. Cell type-specific expression of eicosanoid synthases and receptors in human PDAC.

(**A**) UMAP of a human PDAC scRNA-seq dataset generated by Peng et al., subsetted to exclude adjacent normal samples and annotated by cell type. TNK, T and natural killer cells. (**B**) Dotplot of average and percent expression of select eicosanoid synthases/receptors in each cell type. UMAPs of either eicosanoid (**C**) synthase or (**D**) receptor gene expression. Color intensity indicates the normalized gene expression level for a given gene in each cell. (**E**) Table summarizing inferred cellular sources of eicosanoids based on patterns of synthase expression. (**F**) Co-immunofluorescence for relevant eicosanoid synthases (magenta), stromal markers (αSMA, fibroblasts; CD68, macrophages, yellow), and γactin (blue) highlighting stromal or (**G**) tumor expression. Scale bar, 50 μm.

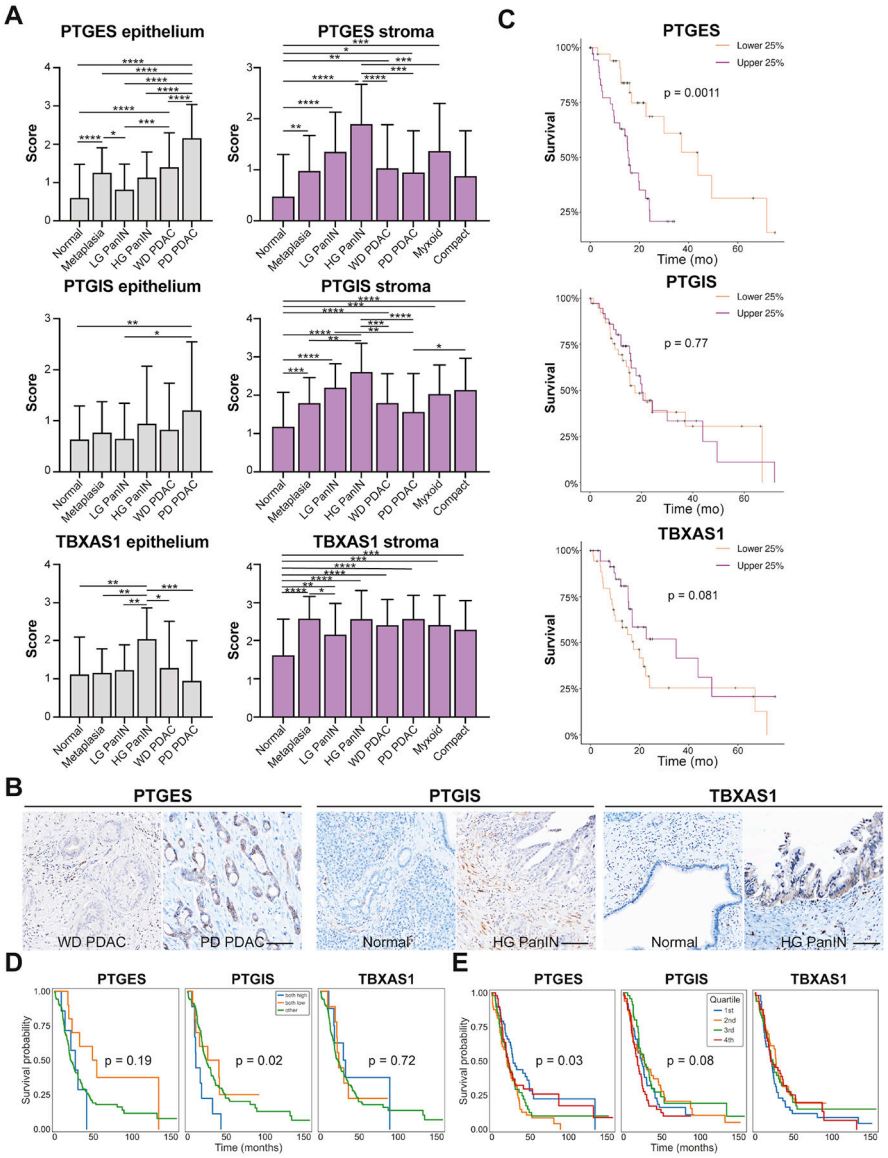

Figure 7. Localization and survival benefit for select eicosanoid synthases in human PDAC.

(**A**) Quantification of scored IHC for PTGES, PTGIS, or TBXAS1 from 22 patients encompassing normal, PanIN, and PDAC-associated stroma and epithelium as well as both myxoid and compact fibrosis. (**B**) Representative IHC images. Scale bar, 100 μm. (**C**) Survival curves for total PTGES, PTGIS, or TBXAS1 expression generated from the TCGA database, representing 150 PDAC patients. The top and bottom 38 patients are shown. Survival curves for (**D**) total (epithelial and stromal expression combined where both high means high expression in both compartments) or (**E**) epithelium specific PTGES, PTGIS, or TBXAS1 expression generated from the Maurer et al., dataset representing 197 epithelial samples and 124 stromal samples from PDAC patients. Quartiles reflect expression broken out into 25% of patients ranked by expression level of a given synthase.